INTERFACE

rsif.royalsocietypublishing.org

Headline review

Cite this article: Löhner A, Cogdell R, Köhler J. 2018 Contribution of low-temperature single-molecule techniques to structural issues of pigment–protein complexes from photosynthetic purple bacteria. *J. R. Soc. Interface* **15**: 20170680.
http://dx.doi.org/10.1098/rsif.2017.0680

Received: 18 September 2017
Accepted: 1 December 2017

Subject Category:
Life Sciences–Physics interface

Subject Areas:
biophysics, chemical biology

Keywords:
low-temperature, single-molecule, pigment–protein complexes, photosynthetic purple bacteria

Author for correspondence:
Jürgen Köhler
e-mail: juergen.koehler@uni-bayreuth.de

Contribution of low-temperature single-molecule techniques to structural issues of pigment–protein complexes from photosynthetic purple bacteria

Alexander Löhner[1], Richard Cogdell[3] and Jürgen Köhler[1,2]

[1]Spectroscopy of Soft Matter, and [2]Bayreuth Institute for Macromolecular Research (BIMF), University of Bayreuth, 95440 Bayreuth, Germany
[3]Institute of Molecular, Cell and Systems Biology, College of Medical Veterinary and Life Sciences, University of Glasgow, Glasgow G12 8QQ, Scotland

JK, 0000-0002-4214-4008

As the electronic energies of the chromophores in a pigment–protein complex are imposed by the geometrical structure of the protein, this allows the spectral information obtained to be compared with predictions derived from structural models. Thereby, the single-molecule approach is particularly suited for the elucidation of specific, distinctive spectral features that are key for a particular model structure, and that would not be observable in ensemble-averaged spectra due to the heterogeneity of the biological objects. In this concise review, we illustrate with the example of the light-harvesting complexes from photosynthetic purple bacteria how results from low-temperature single-molecule spectroscopy can be used to discriminate between different structural models. Thereby the low-temperature approach provides two advantages: (i) owing to the negligible photobleaching, very long observation times become possible, and more importantly, (ii) at cryogenic temperatures, vibrational degrees of freedom are frozen out, leading to sharper spectral features and in turn to better resolved spectra.

1. Introduction

The photosynthetic apparatus of purple bacteria has inspired many researchers, because it represents a relatively simple model system to study the key features of energy- and charge transfer processes in photosynthesis [1–6]. For most of these bacteria one distinguishes a peripheral complex (LH2) and a core complex (RC-LH1) that are associated with the primary photosynthetic processes. The LH2 complexes surround the RC-LH1 complexes in a two-dimensional network and serve as antennas for light harvesting [1,2,7]. Upon optical excitation, the energy is efficiently transferred from LH2 via LH1 to the RC, where it is used to initiate a cyclic electron transfer chain [8,9].

From the X-ray structure of LH2 from *Rhodopseudomonas* (*Rsp.*) *acidophila* it was revealed that this complex is an oligomer of similar building blocks that each accommodates three BChl *a* molecules and one carotenoid [10]. Non-covalent interactions with a pair of αβ-apoproteins properly position the pigments with respect to each other. Depending on the bacterial species, most of these LH2 units form octamers (*Rhodospirillum* (*Rsp.*) *molischianum*) [11] or nonamers (*Rps. acidophila*, *Rhodobacter* (*Rba.*) *sphaeroides*) [10,12,13] in a cylindrical arrangement (figure 1*a*(i)). For the BChl *a* molecules, this results in two pigment pools arranged in concentric rings that are shifted with respect to each other along the common symmetry axis, such that the planes of the rings are perpendicularly oriented with respect to this axis. These two pigment rings are referred to as B800 and B850, according to their room temperature NIR absorption maxima (figure 1*b* top). Depending on the species, the B800 ring consists of eight or nine weakly interacting BChl *a* molecules, whereas the B850 ring features 16 or 18 BChl *a* molecules

THE ROYAL SOCIETY PUBLISHING

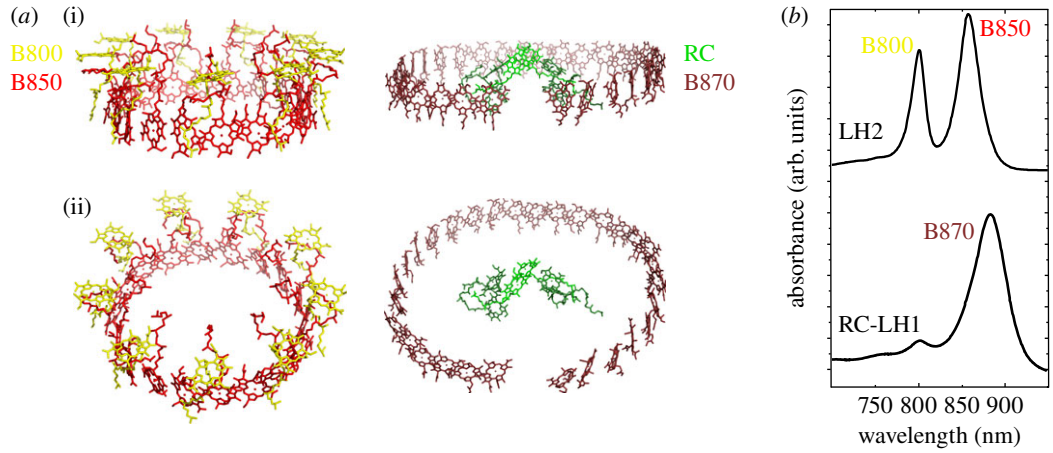

Figure 1. (*a*) Schematic sketch of an assembly of a peripheral LH2 and a core complex (RC-LH1) as side view (i) and as tilted side view (ii). The BChl *a* pigment pools are denoted as B800 (yellow), B850 (red) and B870 (dark red). The pigments of the reaction centre are depicted in green. LH2 from *Rps. acidophila* (PDB-ID: 1NKZ [12]), RC-LH1 from *Rps. palustris* (PDB-ID: 1PYH [14]) rendered with PyMOL [15]. (*b*) Absorption spectra of ensembles of LH2 (top) and RC-LH1 (bottom) complexes from *Rps. acidophila*. Data from [16].

in close contact. Owing to the relatively weak interactions between the B800 BChl *a* molecules, these can be treated in first approximation as independent from each other, although some slight intermolecular coupling has also been discovered between these pigments [17–19]. By contrast, the B850 BChl *a* are much stronger coupled, leading to exciton states, which correspond to delocalized excitations shared by many molecules [4,5,20–23]. The formation of exciton states is accompanied by a redistribution of oscillator strengths, and changes in both the fluorescence lifetime and the spectral positions of the Q_y absorptions. The difference in the electronic coupling strengths between the B800 and B850 pigments explains the striking difference between their corresponding absorptions in the spectra from individual complexes [24]. However, high-resolution structures are available only for a few species of purple bacteria, and many more species exist that show deviations from the 'standard' B800/B850 spectra [16]. It has been generally assumed that these are constructed using a similar modular principle as the LH2 complexes from *Rsp. molischianum* and *Rps. acidophila*, but the detailed structural basis of their BChl assemblies, and, therefore, their spectra, is unknown.

The structural properties of the LH1 complexes are even more complicated. It now appears as if there are at least three different classes of core RC-LH1 complexes. There are two types of monomeric complexes (with and without a gap in the LH1 ring) and dimeric ones [14,25–27]. Initial structural models were based on using homologues of the LH2 building blocks without the B800 BChl *a* molecules [28]. The prediction was then that 16 of these αβ-apoprotein units surround one RC. The resulting pigment pool of 32 BChl *a* molecules is commonly referred to as B870, according to the red-shifted absorption of LH1 with respect to that of LH2 (figure 1*b* bottom).

Information about the geometrical structure of such pigment–protein complexes can be accessed also by optical spectroscopy, which, in general, is sensitive to the electronic structure of the antenna complexes. As the electronic structure is imposed by the underlying geometrical structure, this allows conclusions about subtle structural details to be drawn. However, typical biological samples are heterogeneous and details in the optical spectra might get averaged out in conventional spectroscopy on large ensembles. This can be diminished by both using low temperatures, which reduces thermal broadening effects leading to better resolved spectra, and by studying the proteins individually. Here we will discuss the contribution of low-temperature single-molecule spectroscopy in elucidating details about the electronic structure of the antenna complexes from purple bacteria. This will be illustrated for two examples of LH2 complexes with unusual absorption spectra, followed by two examples of RC-LH1 complexes. Finally, we present an example looking at excitation-energy transfer in a single photosynthetic unit consisting of a single LH2 in close contact with a single RC-LH1 complex.

2. Spectroscopy of single LH2 complexes with unusual absorption spectra

For some species of purple bacteria, depending on the growth conditions, the spectral positions of the absorption bands show deviations from the standard B800/B850 pattern [16]. To understand the relationship between pigment organization and spectral properties, high-resolution structural information is required. Unfortunately, this is available only for two peripheral light-harvesting complexes featuring the standard B800/B850 absorptions (*Rps. acidophila* 10050 and *Rsp. molischianum*) [10–12], and one peripheral light-harvesting complex with an absorption band that is spectrally shifted from 850 to 820 nm (*Rps. acidophila* 7050) [29]. In each of these three cases, the peripheral light-harvesting complexes have a well-defined, homogeneous apoprotein composition. The two types of LH2 complexes of *Rps. acidophila* are often referred to as B800–850 and B800–820 complexes, or sometimes as LH2 and LH3. The B800–820 complex is expressed instead of the B800–850 complex when cells of *Rps. acidophila* are grown under low-light (LL) conditions. From the high-resolution X-ray structures of both peripheral antenna complexes, the standard B800–850 and the LL B800–820 complex, it became clear that most of the spectral shift of the absorption from 850 to 820 nm is the result of the replacement of a few amino acids in the protein backbone that do/do not form hydrogen bonds with the C_3-acetyl group of the B850/B820 BChl *a* molecules, respectively [29].

However, many species have LH2 complexes with strikingly different near-infrared spectra compared to the 'standard' LH2 complexes described above ([16] and references therein). For example, when cells of *Rhodopseudomonas palustris*

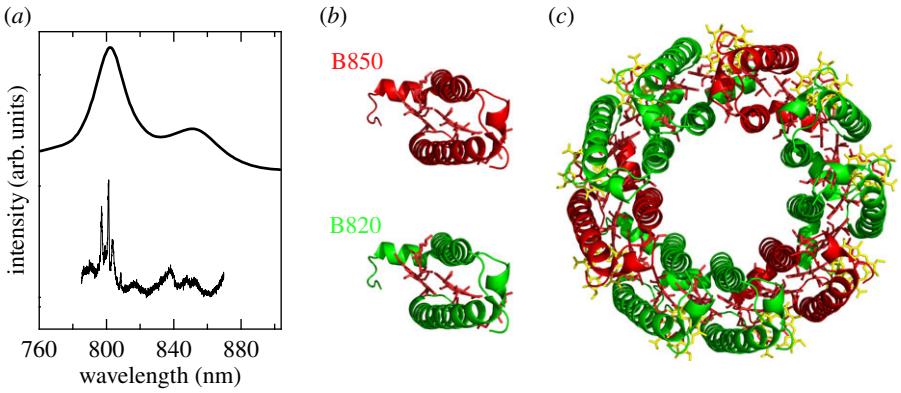

Figure 2. (*a*) Comparison of the absorption spectra from an ensemble of LH2 complexes (top) and an individual LH2 complex (bottom) from *Rps. palustris* grown under LL conditions. Data have been taken from [16,30]. (*b*) X-ray structure of the building blocks of the B800–850 (red), and of the B800–820 (green) peripheral light-harvesting complexes from *Rps. acidophila*. (*c*) Proposed structure for the LL LH2 complex from *Rps. palustris*.

are grown at LL intensity, they produce an LL LH2 complex with an absorption spectrum covering the entire range from 800 to 850 nm; figure 2*a* top, [31–33]. It turned out that for this species the LH2 antennas contain a complex apoprotein composition [34,35]. As some of the *Rps. palustris* apoproteins change the site energies of the 'B850' BChls into a spectral range reminiscent of those BChls of the B800–820 complex from *Rps. acidophila*, the question was raised whether these LH2 complexes consist of rings where each ring has a mixture of apoprotein types. However, using standard ensemble spectroscopy, it would be impossible to distinguish between a mixture of LH2 complexes where each ring is homogeneous but there are various types of rings present, and where each individual ring has a heterogeneous apoprotein composition. A straightforward approach to investigate this question is to use single-molecule techniques.

The fluorescence-excitation spectrum of an individual LL LH2 complex from *Rps. palustris* is shown in the bottom trace of figure 2*a* [30]. The single-complex spectrum features absorption strength over the entire spectral range from 790 to 870 nm. This testifies that LL LH2 from *Rps. palustris* has a heterogeneous apoprotein composition, resulting in BChl molecules with different site energies in one complex. Later, this finding was also confirmed by other methods [36]. This might also explain why it is so difficult to grow high-quality crystals from these proteins. In contrast to the corresponding ensemble-averaged spectrum shown in the top trace of figure 2*a*, the single-complex spectrum reveals rich details, which can be analysed with respect to the spectral separations of the individual bands, and the mutual phase differences of their transition-dipole moments. Doing so for a set of individual complexes yields the distributions of these parameters, which can be used for benchmarking different structural models. Good agreement between the experimental data and computer simulations was obtained for a model that was based on the assumption that the LL LH2 complexes of *Rps. palustris* follow a similar modular construction principle as those complexes from *Rps. acidophila*. Then the known structures of the B850 and B820 building blocks of LH2 from *Rps. acidophila* (figure 2*b*) were used for modelling, and the data could be reproduced for an arrangement of three B850 and six B820 units in a nonameric ring of C_3 symmetry (figure 2*c*, [30]).

Another example for an LH2 complex with an unusual absorption spectrum is that from the species *Allochromatium (Alc.) vinosum* when grown under high-light (HL) conditions

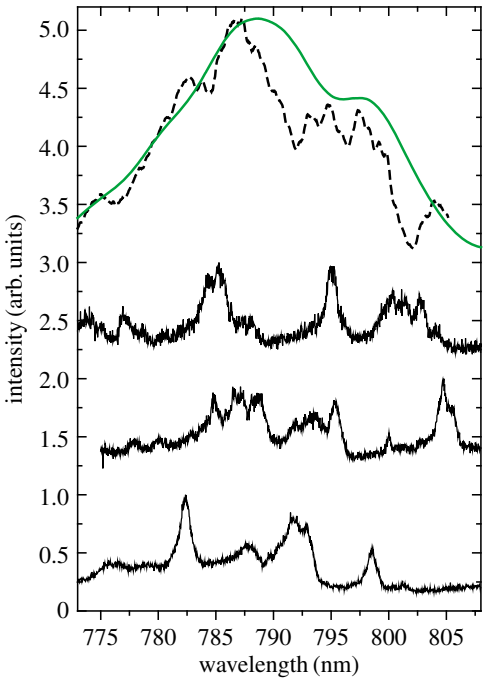

Figure 3. Comparison of several fluorescence-excitation spectra of the B800 spectral region from HL LH2 complexes from *Alc. vinosum*. The top two traces compare the fluorescence-excitation spectrum from an ensemble of LH2 complexes (full green line) and the spectrum that results from summing up 69 spectra from individual LH2 complexes (black dashed line). The lower three traces correspond to spectra from individual complexes. All spectra have been recorded at 1.2 K. Data from [39].

[37,38]. The intriguing feature is that, for this complex, the B800 band is split into two components. Its low-temperature ensemble absorption spectrum is shown by the full green line at the top of figure 3. It features two broad maxima within the B800 spectral region, namely at 789 nm ($B800_{blue}$) and 798 nm ($B800_{red}$) [37,38]. From time-resolved energy transfer studies [38] it was concluded that both B800 bands are present in the same individual LH2 complex. This conclusion was consistent with results obtained by single-molecule spectroscopy [39]. Examples of fluorescence-excitation spectra from the B800 band of individual HL LH2 complexes from *Alc. vinosum* are shown in the lower three traces of figure 3. The spectrum that results from summing up 69 spectra from individual complexes is given by the dashed line at the top of figure 3. For a better comparison it has been overlaid with the ensemble

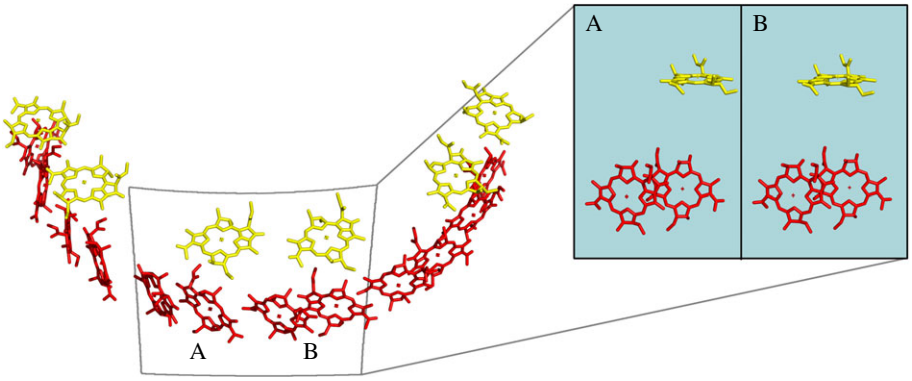

Figure 4. Section of the pigment arrangement used for modelling the spectra from the HL LH2 from *Alc. vinosum*. The inset shows a front view of the two subunits A and B. Figure adapted from [39].

spectrum, testifying that both spectra are in good agreement. The individual spectra, although heterogeneous with respect to the number of bands, spectral positions and spectral bandwidths, each cover the entire range of the B800 region, providing unambiguous evidence that each individual complex contributes to both components of the B800 band.

In contrast to the B800 spectra from *Rps. acidophila* and *Rsp. molischianum*, which featured on average 3–4 absorptions [40,41], the corresponding spectra for HL LH2 from *Alc. vinosum* features on average seven lines [39]. This finding suggested that the LH2 complexes from this species might have larger rings than those from the other two species, which is perfectly in line with results from electron microscopy [37]. Again using the repeat units from *Rps. acidophila* and *Rsp. molischianum* as a starting point for simulating the spectra, best agreement between simulation and experiment was found for a ring-like oligomer of 12 repeat units where the mutual orientation of the B800 and B850 rings resembles that in *Rsp. molischianum*, and where a dimerization of the B800 BChl *a* molecules was taken into account (figure 4 [39]).

The latter implies that in HL LH2 from *Alc. vinosum* the apoprotein arrangement in a single ring must be heterogeneous, which is in agreement with a study of the apoprotein composition that revealed that the α-apoproteins are encoded by three genes [42]. Indeed, the B800 BChl *a* binding motifs present in the α-apoproteins are *molischianum*-like in character but subtly different from each other with respect to the capability of the amino acid residues involved in forming hydrogen bonds with the B800 Bchl *a* molecules. Hence, it was very reasonable to conclude that these differences are at the origin of two types of binding pockets for the B800 BChl *a* molecules causing the above-mentioned dimerization.

Although this yielded a consistent picture, it seems that the assumption of a static protein conformation with dimerized B800 BChl *a* molecules was too simple an approach. Using hole-burning spectroscopy, it has been shown unambiguously that the LL LH2 complex from *Alc. vinosum* undergoes a light-induced conformational change [43]. In single-molecule spectroscopy, a minimum excitation intensity is required to generate a signal that can be discriminated from the background. If this intensity is already sufficient to drive light-induced photophysical/photochemical reactions, then it will not permit the transition between the reaction products to be resolved. However, spectral hole burning also has its inherent limitations. It should be kept in mind that hole-burning spectroscopy averages over objects that have exactly one single spectral property in common—the spectral position of the zero-phonon line. Yet, these objects can still feature large variations in all other properties. This may diminish averaging effects with respect to non-selective ensemble spectroscopies, but it does not avoid averaging of parameters over unknown distributions. Another issue in hole-burning concerns non-resonant excitation of molecules via their phonon sidebands [44]. Whether their contribution is significant or not depends on the electron–phonon coupling strength [45].

In particular for the pigment–protein complexes from purple bacteria, it is known that the electronic coupling between the BChl *a* molecules in the B800 ring leads to electronically excited states that are delocalized over a few, 2–3, individual molecules [17]. This coupling, however, fluctuates on the timescale of seconds, resulting in temporal variations of the spectral positions of the zero-phonon lines [18,46]. Additionally, it has been shown for the pigment–protein complexes from purple bacteria that the electron–phonon coupling strength is also subject to temporal variations [47]. As a consequence of this, the sub-ensemble of proteins that contributes to a hole-burning spectrum is not a static group of objects, but its composition fluctuates in time. Clearly, both techniques, single-molecule spectroscopy and spectral hole burning, have their strengths and weaknesses, but together they can be exploited for obtaining complementary information. Comparing the intensities used in the hole-burning and in the single-molecule experiments, it is clear that for the latter experiments the proteins are driven predominantly into one of the light-induced conformations found in [43]. Nevertheless, from the single-molecule experiments clear evidence is obtained for a heterogeneous apoprotein composition in a single ring (whether driven into an out-of-equilibrium population of the two conformations or not), and the molischianum-like pigment arrangement is confirmed in agreement with the sequence analysis. Given that it takes about 30 s for recording a fluorescence-excitation spectrum from a single complex, it becomes clear that these spectra represent time-averaged spectra. The hole-burning data presented in [43] have been collected from many minutes up to several hours. Hence, these represent averages over both, time and sub-ensembles of fluctuating composition.

As the electronic coupling strength is determined by the ratio of the intermolecular interaction V, and the energy difference between the monomer site energies (diagonal disorder ΔE), which is very sensitive to the local structure of the pigments, fluctuations thereof may be imposed by structural fluctuations of the protein backbone. Then it appears conceivable that the dimerization claimed in [39] is dynamic rather than static. Given the excitation intensity used in the single-molecule

experiments, the situation appears to be static because the proteins are locked into a conformation with distinct electronic couplings among the B800 BChl *a* molecules, giving rise to the observed dimerization. In the hole-burning experiments reported in [43], which are conducted at lower intensities, only a part of the proteins are driven into this conformation. Then the average over the sub-ensemble of proteins, in particular including those that are only exposed briefly to the laser light due to spectral diffusion and/or non-resonant excitation, yields a mixture of dimerized/non-dimerized B800 molecules. This is then observed as a variation of the peak intensity ratio of the two B800 bands as a function of the excitation intensity.

Very recently, the same system has been studied using two-dimensional electronic spectroscopy (D. Zigmantas & R. Cogdell 2017, private communication). There, unambiguous evidence was found that the split B800 band observed for this species reflects an excitonic coupling between dimerized monomers.

3. Spectroscopy of individual RC-LH1 complexes

In recent years, it has become apparent that the discussion of structural issues of RC-LH1 must be very specific with regard to the type of complex and bacterial species under study [14,26,27].

A subtle detail, which, however, is essential for the biological function concerns the debate whether the LH1 ring features a gap or not. This discussion is motivated by the fact that after two light-induced electron transfer steps, a ubiquinone (UQ) in the RC is fully reduced to ubiquinol (UQH_2) [48]. Subsequently, the UQH_2 leaves the RC in order to transfer its reducing equivalents to another protein complex, which is part of the cyclic electron transfer chain [49]. The question is how can the UQH_2 leave the RC and pass through the αβ-apoproteins of the LH1 structure that surround the RC-like palisade [50,51]? The idea that the LH1 structure has a gap was proposed when a protein named pufX was discovered in the LH1 structure of *Rba. sphaeroides* [52]. Interestingly, for this species the core complex is dimeric, consisting of two rings of 15 αβ-apoprotein units enclosing one RC each [26]. This results in an eight-shaped overall structure with two pufX proteins each in the position of the lacking 16th αβ-apoprotein at the nodes. As pufX is essential for photosynthetic growth, and because its position is close to the UQ_b-binding site, it has been argued that it forms a gap through which the UQH_2 can pass [53–55]. This option was further corroborated, when the first low-resolution X-ray structure of an RC-LH1 complex was determined. For *Rps. palustris* the RC-LH1 complex is monomeric, consisting of 15 αβ-apoproteins that enclose the RC in an elliptical arrangement [14]. This complex also features a gap adjacent to the RC UQ_b-binding site (figure 1*a*(ii)), instead of the 16th αβ-apoprotein pair. The gap is filled by a protein termed W, which is believed to be a homologue of pufX. Alternatively, it was proposed that the LH1 structure is a closed ring that is sufficiently flexible to allow the UQH_2 to diffuse through it [56]. Recently, this idea received a boost when the high-resolution X-ray structure of the RC-LH1 complex from *Thermochromatium tepidum* was obtained. Indeed, for this species it was revealed that the RC is surrounded by a closed ring of 16 αβ-apoproteins that form channels on the interface between each pair of adjacent αβ-heterodimers [27]. These authors suggested that this might facilitate the UQH_2 shuttling. Apparently, to make distinct statements about structural properties of the core complex, one has to be specific about the type of RC-LH1 complex under study.

From the perspective of spectroscopy, the presence of a gap in a circular molecular aggregate has severe consequences [57,58]. For a tutorial see appendix. The loss of symmetry leads to a redistribution of the oscillator strength among the exciton states, which is manifested as a relatively narrow feature in the low-energy wing of the absorption spectrum. In figure 5*a*, a typical polarization-resolved fluorescence-excitation spectrum from a single RC-LH1 complex from *Rps. palustris* is shown [58]. Indeed, this allows a narrow peak accompanied by two broad absorptions at higher excitation energies to be distinguished.

The intensities of the three bands are shown on top of the spectra as a function of the polarization of the excitation light. For all three bands the measured intensity variation is compatible with a $\cos^2$ dependence as depicted by the full lines. This reveals that two of the involved transition-dipole moments are approximately parallel with respect to each other and orthogonal with respect to the third one. Closer analysis of the spectra from 44 individual RC-LH1 complexes yields a distribution for the spectral separation between the narrow peak and the broad shoulder next to it, as well as a distribution for the mutual phase difference between the polarization of these two absorptions (figure 5*c*,*d*, light blue entries). Using the crystal structure as a starting point, it was possible to model the distributions of the above-mentioned parameters based on an exciton model. This confirmed the main features of the crystal structure, i.e. an elliptical arrangement with a gap, and also allowed a refinement of the pigment positions [57,58].

In an earlier study on the core complex from *Rps. acidophila*, it appeared difficult to obtain reliable information due to an observed large structural heterogeneity that was ascribed to a large fraction of broken complexes [60]. It was argued that this might be induced at least in part by the experimental procedures. Encouraged by the results obtained on RC-LH1 from *Rps. palustris*, we revisited the core complex from *Rps. acidophila* using a milder detergent for isolating the proteins from the membrane. Indeed, it was found that the fraction of broken complexes could be drastically reduced by replacing lauryldimethylamine *N*-oxide, which was used previously, by the relatively mild detergent dodecyl-β-D-maltoside (DDM) [59]. A typical fluorescence-excitation spectrum of an RC-LH1 complex from *Rps. acidophila* is shown in figure 5*b*. The spectrum resembles that for *Rps. palustris* with respect to the widths of the bands, their mutual spectral positions and their mutual phase differences. This holds true also for the statistics obtained from 61 individual complexes presented in figure 5*c*,*d*, by the red entries. Hence, the spectra of the RC-LH1 complexes from *Rps. palustris* and *Rps. acidophila* are compatible with the same model structure.

Several schemes for immobilization of pigment–protein complexes have been reported in the literature [61–63]. For some species this has led to conflicting results, motivating the need for solution or membrane-based studies. An issue that is often raised in the context of low-temperature single-molecule spectroscopy is that the immobilization of the pigment–protein complexes in a polymer might affect the proteins and may even lead to a disruption of the complexes. Therefore, we undertook to test this and reconstituted both LH2 and RC-LH1 complexes from *Rps. acidophila* into a phospholipid

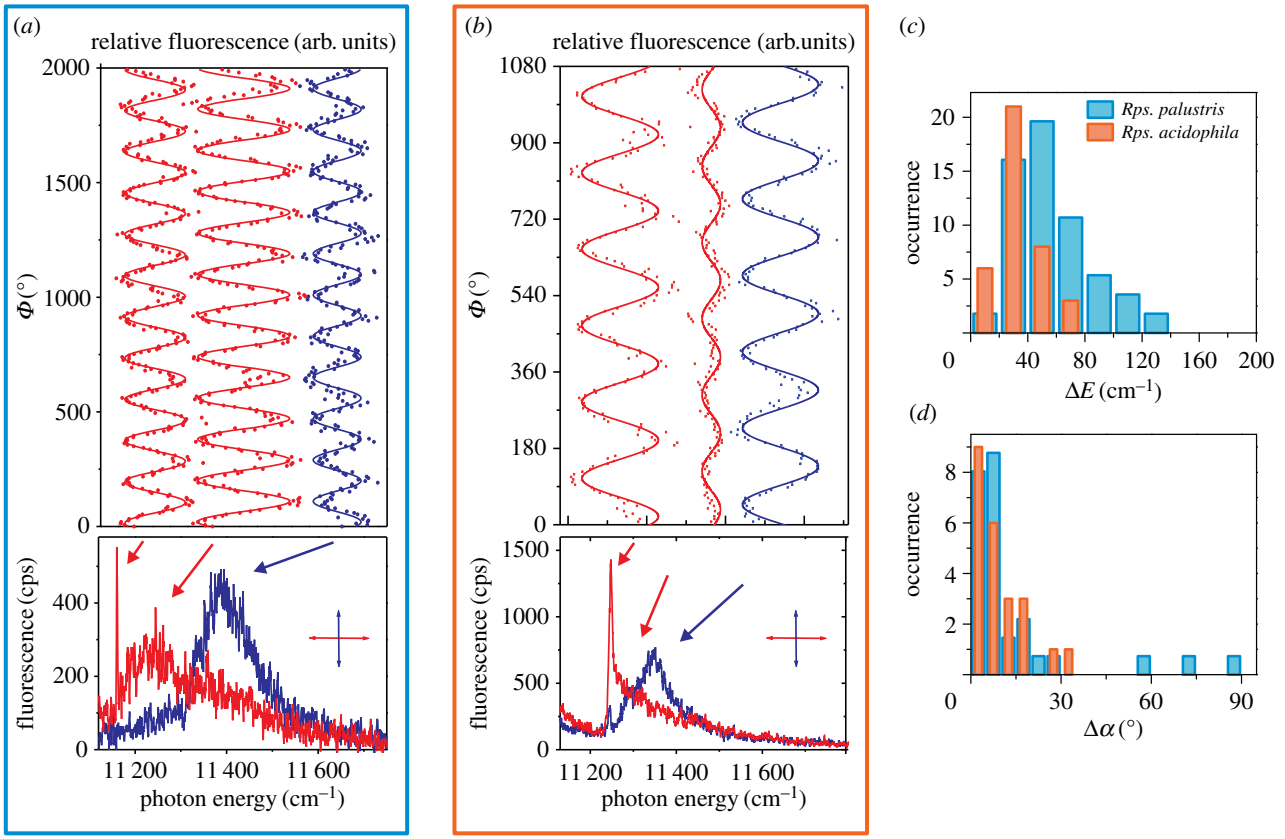

Figure 5. Fluorescence-excitation spectra of an individual RC–LH1 complex from (*a*) *Rps. palustris* and (*b*) *Rps. acidophila* as a function of the polarization of the incident light. The bottom traces show two examples of spectra that have been recorded with mutually orthogonal polarization. The evolution of the intensities of the three bands as a function of the polarization (top panel, dots) is compatible with a $\cos^2$ dependence (full lines). Distributions (*c*) of the spectral separations, and (*d*) the phase differences between the narrow line observed in (*a,b*) and the broad band next to it for *Rps. palustris* (blue) and *Rps. acidophila* (orange). Data from [58,59].

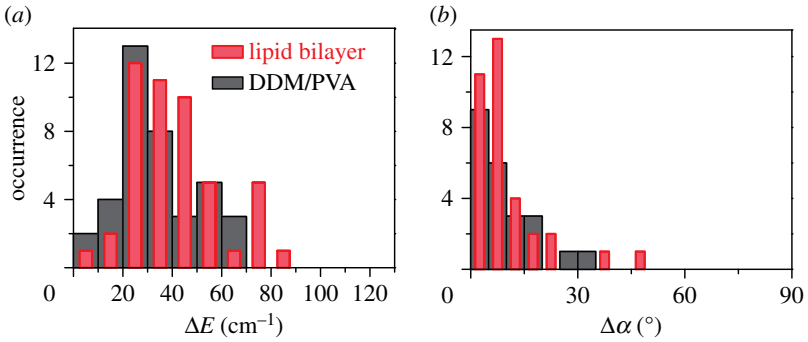

Figure 6. Comparison of the distributions (*a*) of the spectral separations, and (*b*) the phase differences between the narrow line observed and the broad band next to it for *Rps. acidophila* immobilized in DDM/PVA (grey) and reconstituted into a DOPC lipid bilayer (red). Data from [64].

bilayer and compared the results with those obtained from LH complexes immobilized in a polymer [64,65]. Of course, single-molecule spectroscopy cannot solve structures but it allows the distributions of spectral parameters to be obtained rather than their moments only, which is what one would obtain from (sub-) ensemble techniques. Hence, for similar distributions we come to similar conclusions about the underlying structure that results in the observed spectral features. As an example, we illustrate the outcome from the more recent RC-LH1 reconstitution. For the work on LH2 the reader is referred to the literature, yet it is worth noting that the experiments on LH2 in detergent/polymer and those on LH2 reconstituted into a DOPC bilayer yielded identical results [65]. For RC-LH1 from *Rps. acidophila* the distributions of the energetic separations between the narrow spectral feature and the broad band next to it, as well as their mutual phase difference, are shown in figure 6 as a function of the matrix into which the complexes have been embedded. The statistical parameters of these distributions are summarized in table 1. Within statistical limits, the results obtained are identical for both environments, thereby resolving doubts about the sample integrity in a polymer environment. Unfortunately, to the best of our knowledge, a similar study that compares hole-burning data on samples immobilized in glycerol and those reconstituted into a model membrane is still lacking to date.

4. Excitation energy transfer in a single photosynthetic unit

During experiments on individual LH2 complexes from *Rba. sphaeroides*, it happened by serendipity that we observed the

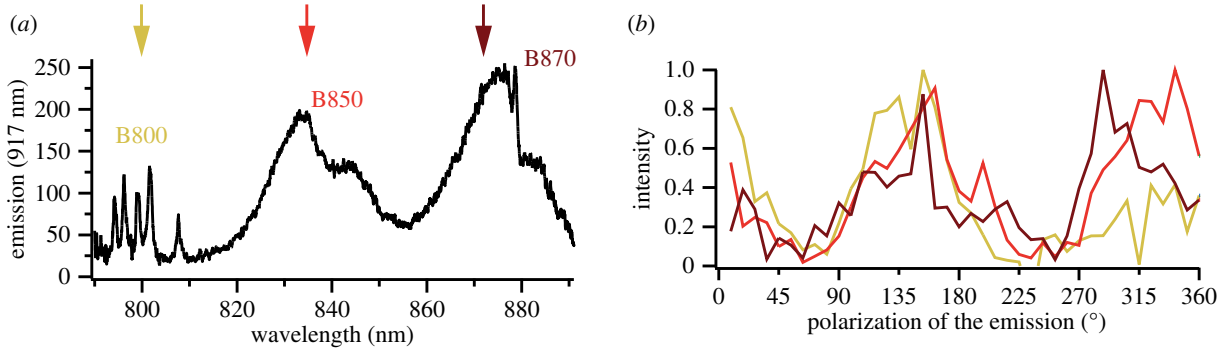

Figure 7. (*a*) Fluorescence-excitation spectrum of a single LH2 complex that is attached to a single RC-LH1 complex from *Rba. sphaeroides*. The spectral regions of the absorptions of the three BChl *a* pigment pools B800 and B850 of LH2 and B870 of LH1 are indicated. The fluorescence was detected at 917 nm. (*b*) Polarization-resolved emission intensity of the single photosynthetic unit for excitation energies in the B800 (yellow), B850 (red) and B870 (dark red) spectral region as indicated by the arrows in (*a*). Data have been taken from [66].

Table 1. Energetic separations, ΔE, of the narrow spectral feature and the broad band next to it, and mutual angles, $\Delta\alpha$, between the corresponding transition-dipole moments for RC–LH1 complexes from *Rps. acidophila* embedded in DDM/PVA or reconstituted into a model membrane, respectively.

	ΔE (mean $\pm$ s.d.)/cm^{-1}	$\Delta\alpha$ (mean $\pm$ s.d.)/°
DDM/PVA[a]	33 $\pm$ 17	8.5 $\pm$ 7.8
DOPC[b]	40 $\pm$ 18	9.4 $\pm$ 9.8

[a]Data from ref. [59].
[b]Data from ref. [64].

spectral signature of a single photosynthetic unit consisting of a single LH2 complex in close contact with a single RC-LH1 complex (figure 7*a*, [66]).

The fluorescence intensity detected from this single photosynthetic unit is shown in figure 7*b* as a function of both the polarization of the emitted radiation and the excitation wavelength, which was chosen to coincide either with the absorption bands of the LH2 complex (B800/B850) or to coincide with the absorption band of the LH1 unit (B870). As a matter of fact, the polarization of the emission does not depend on the excitation wavelength, which testifies the energy transfer from LH2 to LH1. This was a remarkable result because the experiments were carried out under cryogenic conditions on proteins that were immobilized in a polymer matrix. This outcome demonstrates the functionality of this mini-photosynthetic unit at low temperatures in a non-membrane environment.

5. Conclusion

It must be clearly stated that spectroscopy cannot solve structures! Yet, spectroscopy can search for the presence (or lack) of spectral signatures that are characteristic of specific structural features and thereby test whether a proposed structural model is compatible with the experimentally observed spectra. No more, no less! Yet, given the heterogeneity of the biological samples, such distinctive spectral features might get washed out in conventional spectroscopy due to ensemble averaging. This is where low-temperature single-molecule spectroscopy comes into play as an effective tool. The low temperatures diminish thermal broadening effects, which results in a tremendous gain in spectral resolution, and the single-molecule approach avoids ensemble averaging.

However, it should be kept in mind that, to be of added value, this technique requires some prerequisites to be fulfilled. It is trivial to mention but the system under study should fluoresce and should be photostable for some reasonable time interval to allow for the collection of a sufficient number of photons. Obviously, a high-fluorescence quantum yield would be desirable. The signal obtained during the experimental dwell time corresponds to a temporal average, as nicely pointed out in [67]. Hence, if the spectral dynamics that presumably reflects some conformational dynamics is fast with respect to the timescales dictated by experimental constraints, spectral details can get washed out due to temporal averaging. This has been observed, for example, for the Fenna–Matthews–Olson complex from green sulfur bacteria [68]. The single-complex spectra reproduce the ensemble spectrum; in other words, the system behaves ergodic on the experimental timescale. If the spectral dynamics occur on intermediate timescales i.e. fast with respect to the dwell time needed to record a single spectrum yet slow enough to resolve spectral changes between subsequent spectra, it becomes possible to obtain information about conformational dynamics, as has been shown for LH2 [63,69–72], for photosystem I from cyanobacteria [73–76] or for LHC2 from plants [77–80]. In recent years, this methodology has been applied also to study individual chlorosomes, which are the light-harvesting antenna of green sulfur bacteria [81–87]. Chlorosomes are supramolecular assemblies of hundreds of thousands of BChl molecules. Nevertheless, studying single chlorosomes reduces the inherent heterogeneity and, together with theoretical modelling, valuable insights about the internal structure of the chlorosomes could be obtained [88].

At the end of the day, it must be appreciated that all experimental techniques from genetic mutagenesis, crystallography, electron microscopy, magnetic resonance, optical ensemble techniques, sub-ensemble techniques such as hole burning and delta-fluorescence line narrowing, time-resolved spectroscopies, to single-molecule spectroscopy and so on have their pros and cons. There is no unique technique that can provide a single, complete picture. All these methods provide valuable information about the electronic and/or geometric structure of the pigment–protein complexes, and only by combining information from as many techniques as possible can a consistent picture of the structure and function of these proteins be obtained.

Data accessibility. This article has no additional data.

Competing interests. We declare we have no competing interests.

Funding. The authors thank the Deutsche Forschungsgemeinschaft (GRK1640) and Bayerisches Staatsministerium für Bildung und Kultus, Wissenschaft und Kunst (SolTech) for financial support.

Acknowledgements. A.L. and J.K. thank the State of Bavaria for financing the position of A.L. in the framework of the Collaborative Research Network 'Solar Technologies go Hybrid'. Furthermore, we would like to thank our co-workers and collaboration partners who have contributed to this work and whose names are listed in the references.

Appendix

A.1. Exciton states, symmetry and selection rules

For readers who are not familiar with the quantum mechanics required to connect exciton states and symmetry properties, we provide here a brief and simplified outline that should help the reader grasp the essentials without elaborating the detailed mathematical background. For an ideal molecular aggregate (i.e. perfect geometrical order, all molecules identical) the electronic interaction between the monomers leads to electronically excited states that are fully delocalized over the entire aggregate. The strength of this interaction is determined by the geometrical arrangement (distance and orientation) of the monomers with respect to each other. The (quantum mechanical) strategy for determining the proper energies and (eigen-) states of the system is as follows: (i) setup the Hamilton Operator of the system. This is the quantum mechanical operator for the energy. (ii) Find the form in which this operator can be associated with a matrix that is diagonal. (iii) Then the diagonal elements of the matrix correspond directly to the energies of the coupled system and (iv) the transformations required to diagonalize the Hamiltonian provide the proper (eigen-) states of the coupled system. The mathematics is straightforward but would be tedious to go through here, where it is sufficient to just give the results. For a well-ordered geometry, for example, identical monomers equidistantly arranged in a chain or in a ring, the electronically excited states of the aggregate can be calculated as

$$|k\rangle = \frac{1}{\sqrt{N}} \sum_{n=1}^{N} \mathrm{e}^{i2\pi k \frac{n}{N}} |n\rangle. \qquad \text{(A 1)}$$

The meaning of this expression is as follows: N corresponds to the total number of monomers in the aggregate, $|n\rangle$ denotes an electronically excited state localized on monomer n with all other $N-1$ monomers in the electronic ground state. The quantum number k runs from 1 to N. The excited states $|k\rangle$ of the aggregate are obtained by multiplying each of the N local excitations with a factor, and subsequent summation. It is important to realize that the exponentials correspond only to a phase factor, their magnitudes are always equal to 1. Since the phase factors for the k-values $k=0$ ($\mathrm{e}^{i2\pi\cdot 0}=1$) and $k=N$ ($\mathrm{e}^{i2\pi\cdot n}=1$, for any n) yield identical results, it is equivalent to use a numbering scheme where the quantum number k runs from *0* to $N-1$. Similar equivalencies can be found for $k=N-1 \Leftrightarrow k=-1$; $k=N-2 \Leftrightarrow k=-2$; and so on. Therefore, it became common practice for regularly arranged monomers to use the more symmetric boundaries $-N/2 < k \leq N/2$ if N is even and $-(N-1)/2 < k \leq (N-1)/2$ if N is odd. Yet, please be aware that all three numbering schemes yield the same results for the exponentials. The $|k\rangle$ states are called excitons (or Frenkel excitons, molecular excitons) and correspond to excitations that are shared by all monomers in the aggregate. This is because all monomers contribute to the sum in equation (A 1). The exciton states are the elementary electronic excitations of the molecular aggregate. Due to the electronic interaction the initially equal excitation energies of the monomers are transformed into the energies of the exciton states that are spread over the exciton 'band'. For the aggregates that are of relevance in the context of this manuscript, the exciton state with the lowest quantum number (here $k=0$) is lowest in energy.

A.1.1. Transition-dipole moment of the aggregate

Concerning optical spectroscopy the important question is which of the exciton states is accessible by light? Or, in other words: what do the transition-dipole moments $\boldsymbol{M}(k)$ between the exciton states $|k\rangle$ and the electronic ground $|g\rangle$ state look like? According to quantum mechanics, this is given by

$$\boldsymbol{M}(k) = \langle g|\boldsymbol{D}|k\rangle.^{1} \qquad \text{(A 2)}$$

The bracket $\langle g|\boldsymbol{D}|k\rangle$ expresses the quantum mechanical machinery to calculate the transition-dipole moment using the dipole operator $\boldsymbol{D}$. However, the exciton states are superpositions of the localized excitations and inserting equation (A 1) into equation (A 2) yields

$$\boldsymbol{M}(k) = \frac{1}{\sqrt{N}} \sum_{n=1}^{N} \mathrm{e}^{i2\pi k \frac{n}{N}} \underbrace{\langle g|\boldsymbol{D}|k\rangle}_{\boldsymbol{m}(n)} = \frac{1}{\sqrt{N}} \sum_{n=1}^{N} \mathrm{e}^{i2\pi k \frac{n}{N}} \boldsymbol{m}(n), \qquad \text{(A 3)}$$

where the abbreviation $\langle g|\boldsymbol{D}|n\rangle = \boldsymbol{m}(n)$ has been used to denote the transition-dipole moment $\boldsymbol{m}(n)$ of monomer n. Then equation (A 3) simply states that the transition-dipole moment of an exciton state can be obtained as the sum of the monomer transition-dipole moments each multiplied by an appropriate phase factor. Optically allowed transitions are possible only if the individual contributions to the sum interfere constructively. Instead of going through the mathematics we will illustrate the consequences using a pictorial representation, figure 8(*a*), using an artificial molecular aggregate consisting of four monomers arranged in a square. This geometry resembles the arrangement of the BChl molecules in LH1 and LH2 but is easier to grasp because it is a smaller system. Each monomer is envisaged as a small molecular (transition) dipole moment $\boldsymbol{m}$ represented by a black arrow numbered 1–4. For this 'aggregate' we have the localized states $|n\rangle$ with n running from 1–4, and the $|k\rangle$ states $|k=0\rangle$, $|k=1\rangle$, $|k=2\rangle$ and $|k=3\rangle$, where the latter is equivalent to $|k=-1\rangle$ (see numbering schemes above). Using $N=4$, the resulting phase factors $\mathrm{e}^{i2\pi k(n/N)}$ in equation (A 3) are given in table 2 (modulo 2π).

Accordingly, we find for the phase shifts of the monomer transition-dipole moments the values: 0 ($=2\pi$), $\pi/2$, $-\pi/2$ ($=3\pi/2$) and π ($=-\pi$). The extra phase shift is nothing else but a shift in time of the oscillation of the local transition-dipole moment. For the four monomers of our example this is incorporated into figure 8 by the waves connected to each individual monomer, and which represent the contribution of each local transition-dipole moment as a function of time. For example, for the state $|k=0\rangle$ all extra phase factors are equal to 1, and all monomer dipoles oscillate in phase (each with respect to its own local coordinate system), figure 8*a*. Given the geometric arrangement on a square the amplitudes of the monomers 1 and 3 as well as those of 2 and 4 cancel

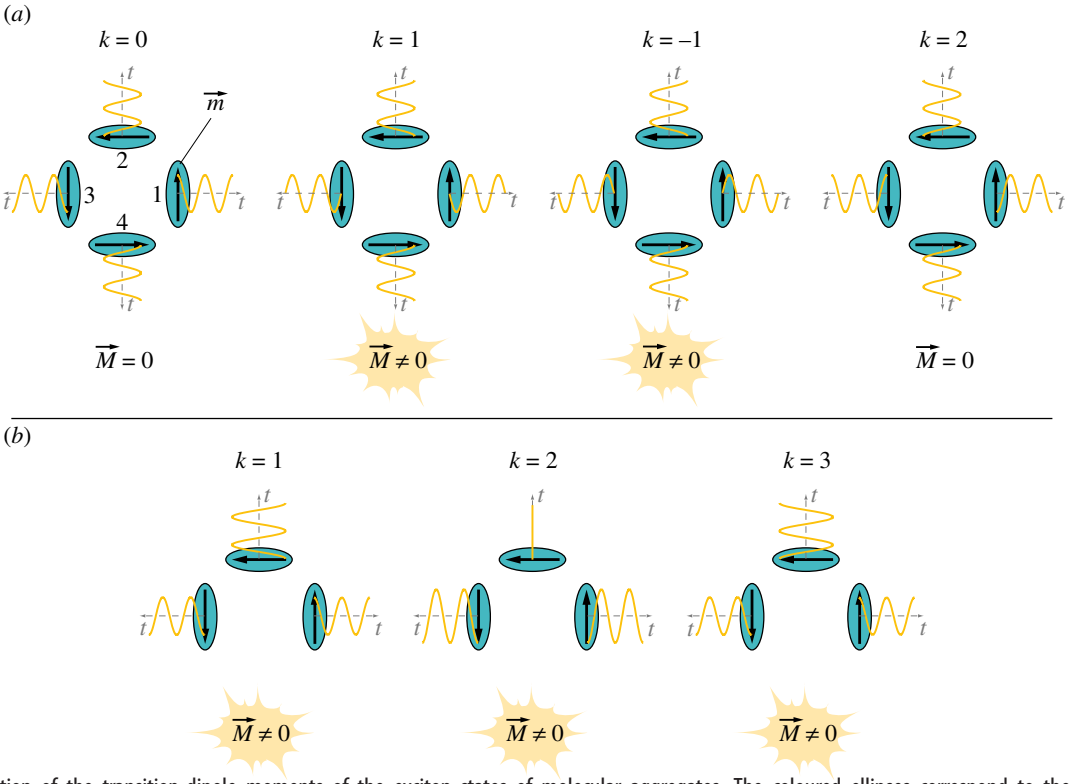

Figure 8. Illustration of the transition-dipole moments of the exciton states of molecular aggregates. The coloured ellipses correspond to the monomers each featuring a transition-dipole moment $\vec{m}$ represented by an arrow that oscillates in time. (*a*) Aggregate of four monomers arranged on a square. For each of the exciton states the monomer transition-dipole moments are multiplied by the respective phase factor given in table 2. Only for the $|\pm 1\rangle$ exciton states the oscillating monomer dipole moments interfere constructively resulting in a net transition-dipole moment $\vec{M}$ of the aggregate. (*b*) Aggregate where one of the monomers has been removed. Now the mutual cancellation of the oscillations of individual transition-dipole moments is lifted and in particular the exciton state lowest in energy (here $|k = 1\rangle$) becomes optically allowed

Table 2. Phase factors in equation (3) as a function of k and n for the example $N = 4$.

k/n	1	2	3	4
$\|k = 0\rangle$	1	1	1	1
$\|k = 1\rangle$	$e^{i\frac{\pi}{2}}$	$e^{i\pi}$	$e^{-i\frac{\pi}{2}}$	$e^{i2\pi}$
$\|k = -1\rangle = \|k = 3\rangle$	$e^{-i\frac{\pi}{2}}$	$e^{i\pi}$	$e^{i\frac{\pi}{2}}$	$e^{i2\pi}$
$\|k = 2\rangle$	$e^{i\pi}$	$e^{i2\pi}$	$e^{i\pi}$	$e^{i2\pi}$

each other, and one obtains $\boldsymbol{M}(k = 0) = 0$ for the net transition-dipole moment of the aggregate in state $|k = 0\rangle$. The same net result is obtained for the state $|k = 2\rangle$, when taking the phase shifts given in the table appropriately into account. The only states where the oscillations of the individual transition-dipole moments interfere constructively are the states $|k = 1\rangle$ and $|k = -1\rangle$, respectively, resulting in a finite transition-dipole moment $\boldsymbol{M}$ for the entire aggregate (figure 8*a*). For the sake of brevity, we will not analyse further the polarizations of the respective transitions, but we note that this information is also available from these considerations.

A.1.2. Introduction of a symmetry-breaking gap

Now consider a situation where one of the monomers has been removed (figure 8(*b*)). The quantum mechanical recipe for calculating the energies and exciton states is still the same as above, yet the expression for their calculation can be given only in very general manner,

$$|k\rangle = \sum_{n=1}^{N} a_n(k)|n\rangle = \sum_{n=1}^{N} |a_n(k)|e^{i\phi_n(k)}|n\rangle \qquad (A\,4)$$

and

$$\text{fulfilling} \quad \sum_{n=1}^{N} |a_n(k)|^2 = 1. \qquad (A\,5)$$

The coefficients are complex numbers, and their magnitudes as well as their phase factors depend on the details of the system under study. In contrast to the fully symmetric case, where each localized state $|n\rangle$ contributed with equal weight (i.e. $1/\sqrt{N}$) to the exciton states and where the mutual phase shifts were multiples of $2\pi/N$, this regularity is lost if the symmetry of the system is reduced. Since the convenient symmetric numbering scheme of the exciton states resulted solely from the symmetry properties of the arrangement this is lost as well, and we have to number the exciton states from 1 to N. Yet, also for this example aggregate the lowest quantum number is associated with the exciton state lowest in energy. The details, namely the magnitudes and phases of the coefficients $a_n(k) = |a_n(k)| \cdot e^{i\phi_n(k)}$ have to be calculated from the Hamiltonian and its transformations. We illustrate this with the example shown at the bottom of figure 8. The monomers are considered to have equal energies and the interaction strength is taken into account only for nearest neighbours. Diagonalization of the corresponding

Hamiltonian yields the following exciton states

$$|k=1\rangle = |n=1\rangle - \frac{1}{\sqrt{2}}|n=2\rangle + |n=3\rangle$$
$$|k=2\rangle = -\frac{1}{\sqrt{2}}|n=1\rangle + \frac{1}{\sqrt{2}}|n=3\rangle \qquad (A\,6)$$
$$|k=3\rangle = |n=1\rangle + \frac{1}{\sqrt{2}}|n=2\rangle + |n=3\rangle.$$

The transition-dipole moments of the exciton states follow from

$$\boldsymbol{M}(k) = \sum_{n=1}^{N} a_n(k) \underbrace{\langle g|\boldsymbol{D}|k\rangle}_{\boldsymbol{m}(n)} = \sum_{n=1}^{N} a_n(k)\, \boldsymbol{m}(n), \qquad (A\,7)$$

which obviously will lead to a very different result with respect to the outcome of equation (A 3). For the example aggregate of three monomers the proper amplitudes and phase shifts of the contributions from the individual transition-dipole moments have been incorporated into figure 8(*b*). In contrast to the symmetric case, now the perfect pairwise cancellations of the contributions from the individual dipole moments for some exciton states are gone and all exciton states feature a net transition-dipole moment $\boldsymbol{M}$. In particular, the exciton state lowest in energy becomes optically accessible upon the introduction of the gap. For more realistic scenarios, i.e. aggregates that feature differences in their site energies (diagonal disorder) and taking also higher-order interactions into account, the maths just gets more elaborate and the coefficients $a_n(k)$ will look more difficult, yet qualitatively the situation remains the same. This reasoning is purely based on symmetry arguments and does not depend on the actual size of the aggregate.

A.1.3. Connection with LH2 and LH1

The transition-dipole moments of the BChl molecules in the B850 of LH2 (closed ring) are oriented mainly in the plane perpendicular to the symmetry axis of the assembly and feature only a small component parallel to this axis. Calculating the exciton states for this assembly yields the well-known ladder numbered $k=0$, $k=\pm1$, ... etc. The transition-dipole moment of the lowest exciton state ($k=0$) results from the parallel components of the monomers, where parallel refers to the symmetry axis of the ring. Its magnitude is small (with respect to the strong in-plane components that result for the $k=\pm1$ states), and its orientation is unfavourable for our optical experiments, because it coincides with the optical axis. Hence, even if the parallel components of the transition-dipole moments would be strong we would not be able to observe it. The situation described so far holds for a perfectly symmetric aggregate. Taking structural/energetic disorder into account mixes the initial exciton states. Due to this mixing, the lowest exciton state obtains some oscillator strength—this explains why the emission stems from this state. 'It borrows intensity' from the highly allowed $k=\pm1$ exciton states. From the $k=\pm1$ states the population relaxes quickly (≈100 fs) to the lowest state. Fast relaxation yields broad bands due to the Heisenberg time–energy uncertainty relation, i.e., for (individual) LH2 complexes in the order of 100 cm^{-1}. The lowest state has a lifetime of about 1 ns, corresponding to a homogeneous linewidth of far less than 0.01 cm^{-1} (at low T) that cannot be resolved. Going through the quantum mechanics, it can be shown that the intensity of the $k=0$ state is stronger the larger the deviations from perfect symmetry. As a consequence, a narrow spectral feature can be observed now and then for LH2, featuring a width of some cm^{-1}. As pointed out above, this is not the intrinsic linewidth but rather an envelope that reflects spectral fluctuations (spectral diffusion) on timescales faster than the time to scan the laser across this transition. However, this occurs rarely; this distinctive spectral feature can only be observed, for at most, 10% of the LH2 complexes studied.

Now let us turn to a ring (of whatever size) with a gap. In contrast to the situation described above for LH2, the lowest exciton state, now referred to as $k=1$ due to the loss of symmetry, is intrinsically allowed without the need to 'borrow intensity'. Again the linewidth is determined by the relaxation time, for LH1 this is about 100 fs for the higher exciton states, and about 300 ps for the lowest one. As before, this yields spectrally broad bands for the higher exciton states and a narrow feature at the red end stemming from the lowest exciton state. Performing experiments under similar conditions as for LH2, we observed this feature in every (!) spectrum from RC-LH1 of *Rps. palustris*, because it was much easier to detect given its stronger intensity. For the linewidths of these transitions values of the order of 1 cm^{-1} have been determined, which still reflects unresolved spectral diffusion. For further reading we refer to [89,90].

A.1.4. Summary

For a closed ring of ideal symmetry the total in-plane transition-dipole moment is zero, and it becomes finite upon introduction of a gap. In the former case, the lowest exciton state can gain oscillator strength only by deviating from the prerequisite of ideal symmetry, for example, by structural and energetic disorder, whereas it becomes intrinsically allowed in the latter case.

Endnote

[1]The reader should not get confused with the use of $|g\rangle$ in the text and $\langle g|$ in the equation. This has a mathematical background that is beyond the scope of this tutorial. For the purpose here this can be ignored.

References

1. Blankenship RE, Madigan MT, Bauer CE. 1995 *Anoxygenic photosynthetic bacteria.* Advances in photosynthesis. Dordrecht, The Netherlands: Kluwer Academic Publishers.
2. Green BR, Parson WW. 2003 *Light-harvesting antennas in photosynthesis.* Dordrecht, The Netherlands: Kluwer Academic Publishers.
3. Hunter CN, Daldal F, Thurnauer MC, Beatty JT. 2008 *The purple phototropic bacteria.* Dordrecht, The Netherlands: Springer Science & Business Media.
4. Hu X, Ritz T, Damjanovic A, Autenrieth, F, Schulten, K. 2002 Photosynthetic apparatus of purple bacteria. *Quart. Rev. Biophys.* **35**, 1–62. (doi:10.1017/S0033583501003754)
5. Mirkovic T, Ostroumov EE, Anna JM, van Grondelle R, Scholes GD. 2017 Light absorption and energy transfer in the antenna complexes of photosynthetic organisms. *Chem. Rev.* **117**, 249–293. (doi:10.1021/acs.chemrev.6b00002)
6. Saer RG, Blankenship RE. 2017 Light harvesting in phototrophic bacteria. Structure and function.

Biochem. J. **474**, 2107–2131. (doi:10.1042/BCJ20160753)

7. Blankenship RE. 2002 *Molecular mechanisms of photosynthesis*. Oxford, UK: Blackwell Science.
8. Pullerits T, Sundström V. 1996 Photosynthetic light-harvesting pigment—protein complexes. Toward understanding how and why. *Acc. Chem. Res.* **29**, 381–389. (doi:10.1021/ar950110o)
9. Zinth W, Wachtveitl J. 2005 The first picoseconds in bacterial photosynthesis—ultrafast electron transfer for the efficient conversion of light energy. *Chem. Phys. Chem.* **6**, 871–880. (doi:10.1002/cphc.200400458)
10. McDermott G, Prince SM, Freer AA, Hawthornthwaite-Lawless AM, Papiz MZ, Cogdell RJ, Isaacs NW. 1995 Crystal structure of an integral membrane light-harvesting complex from photosynthetic bacteria. *Nature* **374**, 517–521. (doi:10.1038/374517a0)
11. Köpke J, Hu X, Muenke C, Schulten K, Michel H. 1996 The crystal structure of the light-harvesting complex II (B800–850) from *Rhodospirillum molischianum*. *Structure* **4**, 581–597. (doi:10.1016/S0969-2126(96)00063-9)
12. Papiz MZ, Prince SM, Howard T, Cogdell RJ, Isaacs NW. 2003 The structure and thermal motion of the B800–850 LH2 complex from *Rps. acidophila* at 2.0Å resolution and 100 K. New structural features and functionally relevant motions. *J. Mol. Biol.* **326**, 1523–1538. (doi:10.1016/S0022-2836(03)00024-X)
13. Walz T, Jamieson SJ, Bowers CM, Bullough PA, Hunter CN. 1998 Projection structures of three photosynthetic complexes from *Rhodobacter sphaeroides*: LH2 at 6 A, LH1 and RC-LH1 at 25 A. *J. Mol. Biol.* **282**, 833–845. (doi:10.1006/jmbi.1998.2050)
14. Roszak AW, Howard TD, Southall J, Gardiner AT, La CJ, Isaacs NW, Cogdell RJ. 2003 Crystal structure of the RC-LH1 core complex from *Rhodopseudomonas palustris*. *Science* **302**, 1969–1972. (doi:10.1126/science.1088892)
15. Schrödinger PyMOL. The PyMOL Molecular Graphics System.
16. Cogdell RJ, Gall A, Köhler J. 2006 The architecture and function of the light-harvesting apparatus of purple bacteria: from single molecules to *in vivo* membranes. *Quart. Rev. Biophys.* **39**, 227–324. (doi:10.1017/S0033583506004434)
17. Hofmann C, Ketelaars M, Matsushita M, Michel H, Aartsma TJ, Köhler J. 2003 Single-molecule study of the electronic couplings in a circular array of molecules: light-harvesting-2 complex from *Rhodospirillum molischianum*. *Phys. Rev. Lett.* **90**, 13004. (doi:10.1103/PhysRevLett.90.013004)
18. Hofmann C, Aartsma TJ, Michel H, Köhler J. 2004 Spectral dynamics in the B800 band of LH2 from *Rhodospirillum molischianum*. A single-molecule study. *New J. Phys.* **6**, 8. (doi:10.1088/1367-2630/6/1/008)
19. Cheng YC, Silbey RJ. 2006 Coherence in the B800 ring of purple bacteria LH2. *Phys. Rev. Lett.* **96**, 28103. (doi:10.1103/PhysRevLett.96.028103)
20. Alden RG, Johnson E, Nagarajan V, Parson WW, Law CJ, Cogdell RJ. 1997 Calculations of spectroscopic properties of the LH2 bacteriochlorophyll–protein antenna complex from *Rhodopseudomonas acidophila*. *J. Phys. Chem. B* **101**, 4667–4680. (doi:10.1021/jp970005r)
21. Sauer K, Cogdell RJ, Prince SM, Freer A, Isaacs NW, Scheer H. 1996 Structure-based calculations of the optical spectra of the LH2 bacteriochlorophyll–protein complex from *Rhodopseudomonas acidophila*. *Photochem. Photobiol.* **64**, 564–576. (doi:10.1111/j.1751-1097.1996.tb03106.x)
22. Wu H-M, Rätsep M, Lee I-J, Cogdell RJ, Small GJ. 1997 Exciton level structure and energy disorder of the B850 ring of the LH2 antenna complex. *J. Phys. Chem. B* **101**, 7654–7663. (doi:10.1021/jp971514w)
23. Matsushita M, Ketelaars M, van Oijen AM, Köhler J, Aartsma TJ, Schmidt, J. 2001 Spectroscopy on the B850 band of individual light-harvesting 2 complexes of *Rhodopseudomonas acidophila* II. Exciton states of an elliptically deformed ring aggregate. *Biophys. J.* **80**, 1604–1614. (doi:10.1016/S0006-3495(01)76133-4)
24. van Oijen AM, Ketelaars M, Köhler J, Aartsma TJ, Schmidt, J. 1999 Unraveling the electronic structure of individual photosynthetic pigment–protein complexes. *Science* **285**, 400–402. (doi:10.1126/science.285.5426.400)
25. Bahatyrova S *et al.* 2004 The native architecture of a photosynthetic membrane. *Nature* **430**, 1058–1062. (doi:10.1038/nature02823)
26. Qian P, Hunter CN, Bullough PA. 2005 The 8.5A projection structure of the core RC-LH1-PufX dimer of *Rhodobacter sphaeroides*. *J. Mol. Biol.* **349**, 948–960. (doi:10.1016/j.jmb.2005.04.032)
27. Niwa S, Yu L-J, Takeda K, Hirano Y, Kawakami T, Wang-Otomo Z-Y, Miki K. 2014 Structure of the LH1–RC complex from *Thermochromatium tepidum* at 3.0 Angström. *Nature* **508**, 228–232. (doi:10.1038/nature13197)
28. Hu X, Schulten K. 1998 Model for the light-harvesting complex I (B875) of *Rhodobacter sphaeroides*. *Biophys. J.* **75**, 683–694. (doi:10.1016/S0006-3495(98)77558-7)
29. McLuskey K, Prince SM, Cogdell RJ, Isaacs NW. 2001 The crystallographic structure of the B800–820 LH3 light-harvesting complex from the purple bacteria *Rhodopseudomonas acidophila* strain 7050. *Biochemistry* **40**, 8783–8789. (doi:10.1021/bi010309a)
30. Brotosudarmo THP, Kunz R, Böhm PS, Gardiner AT, Moulisova V, Cogdell RJ, Köhler, J. 2009 Single-molecule spectroscopy reveals that individual low-light LH2 complexes from *Rhodopseudomonas palustris* 2.1.6. have a heterogeneous polypeptide composition. *Biophys. J.* **97**, 1491–1500. (doi:10.1016/j.bpj.2009.06.034)
31. Hayashi H, Nakano M, Morita S. 1982 Comparative studies of protein properties and bacteriochlorophyll contents of bacteriochlorophyll–protein complexes from spectrally different types of *Rhodopseudomonas palustris*. *J. Biochem.* **92**, 1805–1811. (doi:10.1093/oxfordjournals.jbchem.a134110)
32. Gall A, Robert B. 1999 Characterization of the different peripheral light-harvesting complexes from high- and low-light grown cells from *Rhodopseudomonas palustris*. *Biochemistry* **38**, 5185–5190. (doi:10.1021/bi982486q)
33. van Mourik F, Hawthornthwaite AM, Vonk C, Evans MB, Cogdell RJ, Sundström V, van Grondelle R. 1992 Spectroscopic characterization of the low-light B800–850 light-harvesting complex of *Rhodopseudomonas palustris*, strain 2.1.6. *Biochim. Biophys. Acta.-Bioenerget.* **1140**, 85–93. (doi:10.1016/0005-2728(92)90023-U)
34. Tadros MH, Waterkamp K. 1989 Multiple copies of the coding regions for the light-harvesting B800–850 alpha- and beta-polypeptides are present in the *Rhodopseudomonas palustris* genome. *EMBO J.* **8**, 1303–1308. (doi:10.1002/j.1460-2075.1989.tb03509.x)
35. Tadros MH, Katsiou E, Hoon MA, Yurkova N, Ramji DP. 1993 Cloning of a new antenna gene cluster and expression analysis of the antenna gene family of *Rhodopseudomonas palustris*. *Eur. J. Biochem.* **217**, 867–875. (doi:10.1111/j.1432-1033.1993.tb18315.x)
36. Mascle-Allemand C, Duquesne K, Lebrun R, Scheuring S, Sturgis JN. 2010 Antenna mixing in photosynthetic membranes from *Phaeospirillum molischianum*. *Proc. Natl Acad. Sci. USA* **107**, 5357–5362. (doi:10.1073/pnas.0914854107)
37. Kereïche S, Bourinet L, Keegstra W, Arteni AA, Verbavatz J-M, Boekema EJ, Robert B, Gall A. 2008 The peripheral light-harvesting complexes from purple sulfur bacteria have different 'ring' sizes. *FEBS Lett.* **582**, 3650–3656. (doi:10.1016/j.febslet.2008.09.050)
38. Niedzwiedzki DM, Bína D, Picken N, Honkanen S, Blankenship RE, Holten D, Cogdell RJ. 2012 Spectroscopic studies of two spectral variants of light-harvesting complex 2 (LH2) from the photosynthetic purple sulfur bacterium *Allochromatium vinosum*. *Biochim. Biophys. Acta.-Bioenerget.* **1817**, 1576–1587. (doi:10.1016/j.bbabio.2012.05.009)
39. Löhner A, Carey A-M, Hacking K, Picken N, Kelly S, Cogdell RJ, Köhler, J. 2015 The origin of the split B800 absorption peak in the LH2 complexes from *Allochromatium vinosum*. *Photosynth. Res.* **123**, 23–31. (doi:10.1007/s11120-014-0036-2)
40. van Oijen AM, Ketelaars M, Köhler J, Aartsma TJ, Schmidt, J. 1998 Spectroscopy of single light-harvesting complexes from purple photosynthetic bacteria at 1.2 K. *J. Phys. Chem. B* **102**, 9363–9366. (doi:10.1021/jp9830629)
41. Hofmann C, Michel H, van Heel M, Köhler J. 2005 Multivariate analysis of single-molecule spectra: surpassing spectral diffusion. *Phys. Rev. Lett.* **94**, 195501. (doi:10.1103/PhysRevLett.94.195501)
42. Carey A-M *et al.* 2014 Characterisation of the LH2 spectral variants produced by the photosynthetic purple sulphur bacterium *Allochromatium vinosum*.

Biochim. Biophys. Acta. **1837**, 1849–1860. (doi:10.1016/j.bbabio.2014.07.022)

43. Kell A, Jassas M, Acharya K, Hacking K, Cogdell RJ, Jankowiak R. 2017 Conformational complexity in the LH2 antenna of the purple sulfur bacterium *Allochromatium vinosum* revealed by hole-burning spectroscopy. *J. Phys. Chem. A* **121**, 4435–4446. (doi:10.1021/acs.jpca.7b03188)
44. Jankowiak R, Reppert M, Zazubovich V, Pieper J, Reinot T. 2011 Site selective and single complex laser-based spectroscopies: a window on excited state electronic structure, excitation energy transfer, and electron-phonon coupling of selected photosynthetic complexes. *Chem. Rev.* **111**, 4546–4598. (doi:10.1021/cr100234j)
45. Keil TH. 1965 Shapes of impurity absorption bands in solids. *Phys. Rev.* **140**, A601–A617. (doi:10.1103/PhysRev.140.A601)
46. Baier J, Gabrielsen M, Oellerich S, Michel H, van Heel M, Cogdell RJ, Köhler J. 2009 Spectral diffusion and electron-phonon coupling of the B800 BChl a molecules in LH2 complexes from three different species of purple bacteria. *Biophys. J.* **97**, 2604–2612. (doi:10.1016/j.bpj.2009.07.052)
47. Kunz R, Timpmann K, Southall J, Cogdell RJ, Freiberg A, Köhler J. 2013 Fluctuations in the electron-phonon coupling of a single chromoprotein. *Angew. Chem. Int. Ed.* **52**, 8726–8730. (doi:10.1002/anie.201303231)
48. Feher G, Allen JP, Okamura MY, Rees DC. 1989 Structure and function of bacterial photosynthetic reaction centres. *Nature* **339**, 111–116. (doi:10.1038/339111a0)
49. Petty K, Jackson JB, Dutton PL. 1979 Factors controlling the binding of two protons per electron transferred through the ubiquinone and cytochrome bc2 segment of *Rhodopseudomonas sphaeroides* chromatophores. *Biochim. Biophys. Acta. Bioenerget.* **546**, 17–42. (doi:10.1016/0005-2728(79)90167-1)
50. Cogdell RJ, Fyfe PK, Barrett SJ, Prince SM, Freer AA, Isaacs NW, McGlynn P, Hunter CN. 1996 The purple bacterial photosynthetic unit. *Photosynth. Res.* **48**, 55–63. (doi:10.1007/BF00040996)
51. Fotiadis D, Qian P, Philippsen A, Bullough PA, Engel A, Hunter CN. 2004 Structural analysis of the reaction center light-harvesting complex I photosynthetic core complex of *Rhodospirillum rubrum* using atomic force microscopy. *J. Biol. Chem.* **279**, 2063–2068. (doi:10.1074/jbc.M310382200)
52. Barz WP, Vermeglio A, Francia F, Venturoli GB, Melandri BA, Oesterhelt D. 1995 Role of the PufX protein in photosynthetic growth of *Rhodobacter sphaeroides*.2. PufX is required for efficient ubiquinone/ubiquinol exchange between the reaction center QB site and the cytochrome bc_1 complex. *Biochemistry* **34**, 15 248–15 258. (doi:10.1021/bi00046a033)
53. Stahl AD, Crouch LI, Jones MR, van Stokkum IHM, van Grondelle, R, Groot ML. 2011 Role of PufX in photochemical charge separation in the RC-LH1 complex from *Rhodobacter sphaeroides*: an ultrafast mid-IR pump-probe investigation. *J. Phys. Chem. B* **116**, 434–444. (doi:10.1021/jp206697k)
54. Sener M, Hsin J, Trabuco LG, Villa E, Qian P, Hunter CN, Schulten, K. 2009 Structural model and excitonic properties of the dimeric RC-LH1-PufX complex from *Rhodobacter sphaeroides*. *Chem. Phys.* **357**, 188–197. (doi:10.1016/j.chemphys.2009.01.003)
55. Qian P, Papiz MZ, Jackson PJ, Brindley AA, Ng IW, Olsen JD, Dickman MJ, Bullough PA, Hunter CN. 2013 Three-dimensional structure of the *Rhodobacter sphaeroides* RC-LH1-PufX complex: dimerization and quinone channels promoted by PufX. *Biochemistry* **52**, 7575–7585. (doi:10.1021/bi4011946)
56. Aird A, Wrachtrup J, Schulten K, Tietz C. 2007 Possible pathway for ubiquinone shuttling in *Rhodospirillum rubrum* revealed by molecular dynamics simulation. *Biophys. J.* **92**, 23–33. (doi:10.1529/biophysj.106.084715)
57. Richter MF *et al.* 2007 Symmetry matters for the electronic structure of core complexes from *Rhodopseudomonas palustris* and *Rhodobacter sphaeroides* $PufX^{-}$. *Proc. Natl Acad. Sci. USA* **104**, 6661–6665. (doi:10.1073/pnas.0611115104)
58. Richter MF, Baier J, Southall J, Cogdell RJ, Oellerich S, Köhler J. 2007 Refinement of the X-ray structure of the RC LH1 core complex from *Rhodopseudomonas palustris* by single-molecule spectroscopy. *Proc. Natl Acad. Sci. USA* **104**, 20 280–20 284. (doi:10.1073/pnas.0704599105)
59. Böhm PS, Southall J, Cogdell RJ, Köhler, J. 2013 Single-molecule spectroscopy on RC-LH1 complexes of *Rhodopseudomonas acidophila* strain 10050. *J. Phys. Chem. B* **117**, 3120–3126. (doi:10.1021/jp4005218)
60. Ketelaars M, Hofmann C, Köhler J, Howard TD, Cogdell RJ, Schmidt, J, Aartsma TJ. 2002 Spectroscopy on individual light-harvesting 1 complexes of *Rhodopseudomonas acidophila*. *Biophys. J.* **83**, 1701–1715. (doi:10.1016/S0006-3495(02)73938-6)
61. Ying, L, Xie XS. 1998 Fluorescence spectroscopy, exciton dynamics, and photochemistry of single allophycocyanin trimers. *J. Phys. Chem. B* **102**, 10 399–10 409. (doi:10.1021/jp983227d)
62. Novoderezhkin VI, Rutkauskas D, van Grondelle R. 2006 Dynamics of the emission spectrum of a single LH2 complex: interplay of slow and fast nuclear motions. *Biophys. J.* **90**, 2890–2902. (doi:10.1529/biophysj.105.072652)
63. Schlau-Cohen GS, Wang Q, Southall J, Cogdell RJ, Moerner WE. 2013 Single-molecule spectroscopy reveals photosynthetic LH2 complexes switch between emissive states. *Proc. Natl Acad. Sci. USA* **110**, 10 899–10 903. (doi:10.1073/pnas.1310222110)
64. Böhm PS, Kunz R, Southall J, Cogdell RJ, Köhler J. 2013 Does the reconstitution of RC-LH1 complexes from *Rhodopseudomonas acidophila* strain 10050 into a phospholipid bilayer yield the optimum environment for optical spectroscopy? *J. Phys. Chem. B* **117**, 15 004–15 013. (doi:10.1021/jp409980k)
65. Richter MF, Baier J, Cogdell RJ, Köhler J, Oellerich S. 2007 Single-molecule spectroscopic characterization of light-harvesting 2 complexes reconstituted into model membranes. *Biophys. J.* **93**, 183–191. (doi:10.1529/biophysj.106.103606)
66. Hofmann C, Francia F, Venturoli G, Oesterhelt D, Köhler J. 2003 Energy transfer in a single self-aggregated photosynthetic unit. *FEBS Lett.* **546**, 345–348. (doi:10.1016/S0014-5793(03)00623-9)
67. Jang S, Silbey RJ. 2003 Theory of single molecule line shapes of multichromophoric macromolecules. *J. Chem. Phys.* **118**, 9312–9323. (doi:10.1063/1.1569239)
68. Löhner A, Ashraf K, Cogdell RJ, Köhler J. 2016 Fluorescence-excitation and emission spectroscopy on single FMO complexes. *Sci. Rep.* **6**, 31875. (doi:10.1038/srep31875)
69. Hofmann C, Aartsma TJ, Michel H, Köhler J. 2003 Direct observation of tiers in the energy landscape of a chromoprotein: a single-molecule study. *Proc. Natl Acad. Sci. USA* **100**, 15 534–15 538. (doi:10.1073/pnas.2533896100)
70. Gall A, Ilioaia C, Krüger, Tjaart PJ, Novoderezhkin VI, Robert B, van Grondelle R. 2015 Conformational switching in a light-harvesting protein as followed by single-molecule spectroscopy. *Biophys. J.* **108**, 2713–2720. (doi:10.1016/j.bpj.2015.04.017)
71. Schörner M, Beyer SR, Southall J, Cogdell RJ, Köhler J. 2015 Multi-level, multi time-scale fluorescence intermittency of photosynthetic LH2 complexes: a precursor of non-photochemical quenching? *J. Phys. Chem. B* **119**, 13 958–13 963. (doi:10.1021/acs.jpcb.5b06979)
72. Schörner M, Beyer SR, Southall J, Cogdell RJ, Köhler J. 2015 Conformational memory of a protein revealed by single-molecule spectroscopy. *J. Phys. Chem. B* **119**, 13 964–13 970. (doi:10.1021/acs.jpcb.5b07494)
73. Jelezko F, Tietz C, Gerken U, Wrachtrup J, Bittl R. 2000 Single-molecule spectroscopy on photosystem I pigment–protein complexes. *J. Phys. Chem. B* **104**, 8093–8096. (doi:10.1021/jp001332t)
74. Brecht M, Radics V, Nieder JB, Studier H, Bittl R. 2008 Red antenna states of photosystem I from *Synechocystis* PCC 6803. *Biochemistry* **47**, 5536–5543. (doi:10.1021/bi800121t)
75. Brecht M, Hussels M, Schlodder E, Karapetyan NV. 2012 Red antenna states of photosystem I trimers from *Arthrospira platensis* revealed by single-molecule spectroscopy. *Biochim. Biophys. Acta.* **1817**, 445–452. (doi:10.1016/j.bbabio.2011.11.012)
76. Skandary S, Konrad A, Hussels M, Meixner AJ, Brecht M. 2015 Orientations between red antenna states of photosystem I monomers from *Thermosynechococcus elongatus* revealed by single-molecule spectroscopy. *J. Phys. Chem. B* **119**, 13 888–13 896. (doi:10.1021/acs.jpcb.5b04483)
77. Tietz C, Jelezko F, Gerken U, Schuler S, Schubert A, Rogl H, Wrachtrup J. 2001 Single molecule spectroscopy on the light-harvesting complex II of higher plants. *Biophys. J.* **81**, 556–562. (doi:10.1016/S0006-3495(01)75722-0)

78. Krüger TPJ, Novoderezhkin VI, Ilioaia C, van Grondelle R. 2010 Fluorescence spectral dynamics of single LHCII trimers. *Biophys. J.* **98**, 3093–3101. (doi:10.1016/j.bpj.2010.03.028)
79. Krüger TPJ, Ilioaia C, Valkunas L, van Grondelle R. 2011 Fluorescence intermittency from the main plant light-harvesting complex: sensitivity to the local environment. *J. Phys. Chem. B* **115**, 5083–5095. (doi:10.1021/jp109833x)
80. Schlau-Cohen GS, Yang H-Y, Krüger TPJ, Xu P, Gwizdala M, van Grondelle R, Croce R, Moerner WE. 2015 Single-molecule identification of quenched and unquenched states of LHCII. *J. Phys. Chem. Lett.* **6**, 860–867. (doi:10.1021/acs.jpclett.5b00034)
81. Furumaki S, Vacha F, Habuchi S, Tsukatani Y, Bryant DA, Vacha, M. 2011 Absorption linear dichroism measured directly on a single light-harvesting system: the role of disorder in chlorosomes of green photosynthetic bacteria. *JACS* **133**, 6703–6710. (doi:10.1021/ja111475z)
82. Tian Y, Camacho R, Thomsson D, Reus M, Holzwarth AR, Scheblykin IG. 2011 Organization of bacteriochlorophylls in individual chlorosomes from *Chlorobaculum tepidum* studied by 2-dimensional polarization fluorescence microscopy. *JACS* **133**, 17 192–17 199. (doi:10.1021/ja2019959)
83. Furumaki S, Yabiku Y, Habuchi S, Tsukatani Y, Bryant DA, Vacha M. 2012 Circular dichroism measured on single chlorosomal light-harvesting complexes of green photosynthetic bacteria. *J. Phys. Chem. Lett.* **3**, 3545–3549. (doi:10.1021/jz301671p)
84. Shibata Y, Saga Y, Tamiaki H, Itoh S. 2006 Low-temperature fluorescence from single chlorosomes, photosynthetic antenna complexes of green filamentous and sulfur bacteria. *Biophys. J.* **91**, 3787–3796. (doi:10.1529/biophysj.106.084178)
85. Shibata Y, Saga Y, Tamiaki H, Itoh S. 2007 Polarized fluorescence of aggregated bacteriochlorophyll *c* and baseplate bacteriochlorophyll a in single chlorosomes isolated from *Chloroflexus aurantiacus*. *Biochemistry* **46**, 7062–7068. (doi:10.1021/bi0623072)
86. Jendrny M, Aartsma TJ, Köhler J. 2012 Fluorescence excitation spectra from individual chlorosomes of the green sulfur bacterium *Chlorobaculum tepidum*. *J. Phys. Chem. Lett.* **3**, 3745–3750. (doi:10.1021/jz301808h)
87. Jendrny M, Aartsma TJ, Köhler J. 2014 Insights into the excitonic states of individual chlorosomes from *Chlorobaculum tepidum*. *Biophys. J.* **106**, 1921–1927. (doi:10.1016/j.bpj.2014.03.020)
88. Günther LM, Jendrny M, Bloemsma EA, Tank M, Oostergetel GT, Bryant DA, Knoester J, Köhler J. 2016 Structure of light-harvesting aggregates in individual chlorosomes. *J. Phys. Chem. B.* **120**, 5367–5376. (doi:10.1021/acs.jpcb.6b03718)
89. Aartsma TJ, Köhler J. 2008 Optical spectroscopy of individual light-harvesting complexes. In *Biophysical techniques in photosynthesis* (eds TJ Aartsma, J Matysik), pp. 241–266. Advances in Photosynthesis and Respiration, vol 2. Dordrecht, The Netherlands: Springer.
90. Cogdell RJ, Köhler J. 2010 Sunlight, purple bacteria and quantum mechanics: how purple bacteria harness quantum mechanics for efficient light harvesting. In *Quantum efficiency in complex systems. Part I: biomolecular systems* (eds ER Weber, M Thorwart, U Würfel), pp. 77–94. Semiconductors and Semimetals, vol. 83. Berkeley, CA: University of California, Academic Press.